Electrochemical and In Situ Scanning Tunneling Microscopy Studies of Submonolayer Deposition of Antimony on Au(100) in Perchloric Acid Solution

Masanori Hara,[†] Junji Inukai,[†,‡] Soichiro Yoshimoto,[†] and Kingo Itaya*[,†,§]

Department of Applied Chemistry, Graduate School of Engineering, Tohoku University, 6-6-04 Aoba, and New Industry Creation Hatchery Center, Tohoku University, 6-6-10 Aoba, Sendai 980-8579, Japan, and Core Research Evolutional Science and Technology organized by Japan Science and Technology Agency (CREST-JST), Kawaguchi Center Building, 4-1-8 Honcho, Kawaguchi, Saitama 332-0012, Japan

Received: June 2, 2004; In Final Form: July 30, 2004

Adlayers of Sb species on Au(100) were investigated in 0.1 M $HClO_4$. Using in situ scanning tunneling microscopy, it was found that irreversibly adsorbed oxygenous Sb(III) species formed a quasi (2×2) structure on Au(100). These species underwent redox reactions on the surface without desorption. In an $HClO_4$ solution containing Sb_2O_3, two adlayers of Sb, $\begin{pmatrix} 1 & 1 \\ -1 & 2 \end{pmatrix}$ and $\begin{pmatrix} 2 & 1 \\ -2 & 2 \end{pmatrix}$, were found. Comparison between the voltammograms recorded in $HClO_4 + Sb_2O_3$ with and without H_2O_2 showed that the H_2O_2 reduction reaction is not enhanced on the adlayer of irreversibly adsorbed oxygenous Sb(III) species but it can be enhanced on the submonolayer of Sb(0).

Introduction

The electroreduction of O_2 is one of the most important reactions in electrochemistry because of its central role in fuel cells, corrosion, and other industrial processes.[1] The complex kinetics of the electroreduction process has been studied for several decades. In acid solution, oxygen reduction proceeds by two pathways depending on the electrode composition. One is a direct four-electron pathway, as shown in eq 1. The other

$$O_2 + 4H^+ + 4e^- \rightarrow 2H_2O \quad (1)$$

is a two-electron pathway with peroxide as the intermediate, as shown in eqs 2 and 3

$$O_2 + 2H^+ + 2e^- \rightarrow H_2O_2 \quad (2)$$

$$H_2O_2 + 2H^+ + 2e^- \rightarrow 2H_2O \quad (3)$$

For example, on Pt and Ag surfaces, oxygen reduction proceeds by the four-electron pathway, whereas on the Au surface, the two-electron process dominates and peroxide is produced.[2,3] In both cases, the cleavage of the oxygen bond seems to be rate determining. The high dissociation energy of O_2, 494 kJ mol^{-1}, leads to slow kinetics and a large overpotential for the four-electron pathway, even on Pt.[4] A substantial overpotential is required for the reduction of peroxide on materials such as Au, even though the O−O bond dissociation energy of H_2O_2, 146 kJ mol^{-1}, is considerably lower than that of O_2.[4]

Foreign metal overlayers formed by underpotential deposition (UPD) may cause considerable changes in the electrochemical activity of electrode surfaces,[5−7] leading to positive or negative catalytic effects depending on the substrate as well as the adsorbate metal. Electrochemical measurements revealed that UPD adlayers of Bi,[5−8] Pb,[5−7,9−13] and Tl[6,7,12−14] considerably accelerate the electroreduction of H_2O_2 and O_2 on Au surfaces. On the basis of electrochemical measurements, it was reported that Au electrodes with fractional coverages of those metal adlayers were significantly more active than either the bare or the monolayer-covered Au surface toward the reduction of H_2O_2 and O_2.[5−11]

Several in situ techniques have been used to understand the relationship between the electrocatalytic activity and structure of UPD overlayers: The adlayer structures of Pb,[15−17] Bi,[18−25] and Tl[26,27] on Au(111), and Pb[28] on Au(100) were studied using in situ scanning tunneling microscopy (STM), atomic force microscopy (AFM), and surface X-ray scattering (SXS). Itaya's group studied the structures of UPD adlayers of Cu on Au(111)[29] and Pt(111)[30] using in situ STM. They also studied the O_2 reduction on Cu-deposited electrodes and found that the configuration of adsorbed O_2 molecules depended on the substrate and the structure of the Cu adlayers.[31,32] Those results obtained by in situ techniques provide direct insight into the relationship between surface structure and electrocatalytic activity. Recently, Li and Gewirth examined the mechanism of the H_2O_2 electroreduction on Bi-submonolayer-modified Au(111) surface using density function theory (DFT) calculations.[4] They suggested that the O atoms in H_2O_2 interact strongly with two Bi atoms and that cleavage of the O−O bond arises because of the distance between adjacent Bi adatoms on the Au(111) surface. As the distance between Bi adatoms decreases with increasing coverage, H_2O_2 can be adsorbed on Bi without breakage of the O−O bond.

The electrodeposition of Sb on Au surfaces is interesting in that oxygenous Sb(III) species, possibly SbO^+,[33,34] were suggested to be adsorbed on the Au electrode irreversibly at potentials more anodic than the UPD potential.[33−37] Electrochemical and STM measurements for the electrochemical deposition of Sb on Au(111) have been carried out by Rhee's group[34] and Mao's group.[35,36] Recently, the adsorption process of irreversibly adsorbed Sb on Au(111) was investigated in detail

* Corresponding author. E-mail: itaya@atom.che.tohoku.ac.jp. Phone/Fax: +81-22-214-5380.
[†] Graduate School of Engineering.
[‡] New Industry Creation Hatchery Center.
[§] CREST-JST.

10.1021/jp047621p CCC: $27.50
Published on Web 10/16/2004

by in situ STM.[33] Yan and co-workers carried out in situ STM studies on the UPD of Sb on Au(100) in H_2SO_4.[37] However, the influence of an electrochemically deposited Sb adlayer on electrocatalytic activity of the Au surface for H_2O_2 reduction has not been reported.[33−37]

In this paper, we report the structure of the adlayer of Sb species on Au(100) in $HClO_4$. At potentials more anodic than the UPD potential, oxygenous Sb(III) species irreversibly formed an adlayer with a quasi (2×2) structure. After the UPD, two adlayer structures of Sb, $\begin{pmatrix} 1 & 1 \\ -1 & 2 \end{pmatrix}$ and $\begin{pmatrix} 2 & 1 \\ -2 & 2 \end{pmatrix}$, were found. On the Au(100) surface, the relationship between the adlayer structure and the reactivity of H_2O_2 was examined in the $HClO_4$ solution.

Experimental Section

Single-crystal electrodes of gold were prepared by the method of Clavilier et al.[38] Briefly, a pure Au wire (0.7 mm in diameter) was melted in a hydrogen flame to form a single-crystal bead. A well-prepared single-crystal bead showed eight facets of (111) in an octahedral configuration and six facets of (100) in a hexahedral configuration. These facets usually exhibited a wide, atomically flat terrace-step structure. For STM observations, one of the (100) facets was directly used. For cyclic voltammetric (CV) measurements, the (100) surface was mechanically exposed and polished with successively finer grades of Al_2O_3 powder, from 1 to 0.3 μm in diameter. The final treatment, performed to expose a clean and ordered surface, consisted of flame annealing, slow cooling in a stream of hydrogen gas, and immersion in ultrapure water. The Au electrode was then transferred into the STM or electrochemical cell with a drop of water protecting the surface from contamination. To reduce the number of small monatomic islands on the Au(100) surface formed after quenching,[39] the electrode potential of the samples placed in both electrochemical and STM cells was kept at 0.9 V vs a reversible hydrogen electrode (RHE) for 20 min before experiments to enhance the Au diffusion on the surface.

Electrochemical STM imaging was performed with a Nanoscope E (Digital Instruments, Santa Barbara, CA). The STM tip was made from a W wire (0.25 mm in diameter) electrochemically etched in 1 M KOH. The tip was then coated with transparent nail polish to minimize the faradaic current. All STM images were taken in the constant-current mode.

All electrolyte solutions were prepared with ultrapure $HClO_4$ (Cica-Merck), 99.9% Sb_2O_3 (Aldrich Chemicals), and ultrapure water (Millipore-Q). All electrode potentials are reported with respect to RHE in 0.1 M $HClO_4$.

Results and Discussion

Cyclic Voltammograms for Sb Deposition. Solution chemistry suggests that the dominant species formed by dissolving Sb_2O_3 in acidic solution (pH 0−1) is SbO^+.[40] In has also been reported that oxygenous Sb(III) species, possibly SbO^+ [36], are adsorbed directly from the acidic solution on the Au electrode irreversibly at potentials more anodic than the UPD potential.[33−36] To investigate the irreversibly adsorbed Sb layer, a CV was recorded on the Au(100) surface in 0.1 M $HClO_4$ (Figure 1a), which had been prepared by immersing a Au(100) electrode into a 50 μM Sb_2O_3 + 0.1 M $HClO_4$ solution at 0.4 V for 1 min and subsequently rinsing with ultrapure water. The prolonged period of immersion, longer than 1 min, did not affect the CV. The electrode potential was first swept negatively from 0.5 V in pure $HClO_4$, and then, the direction of the potential scan was reversed at 0.2 V. The redox peaks of adsorbed oxygenous Sb species (hereafter called SbO^+) were seen at 0.40 V, and the amount of charge consumed for these peaks was 135 μC cm^{-2}. Assuming that SbO^+ adsorbed on Au(100) was transformed into Sb^0, the coverage of irreversibly adsorbed SbO^+ on the Au(100) surface was calculated to be 0.24. The redox peaks of adsorbed SbO^+ were observed reproducibly during the potential cycle between 0.5 and 0.2 V, indicating that SbO^+ remained on the surface in this potential range. Rhee's group and Mao's group reported CVs obtained in H_2SO_4 on Au(100) modified with SbO^+.[33,37] The shapes of their CVs in H_2SO_4 were similar to ours showing a single pair of redox peaks, but the coverage of SbO^+ in their experiment was reported to be 0.33, which is larger by 30% than that of ours in $HClO_4$. A large influence of (bi)sulfate ions[36] is also seen in the following case of the UPD of Sb.

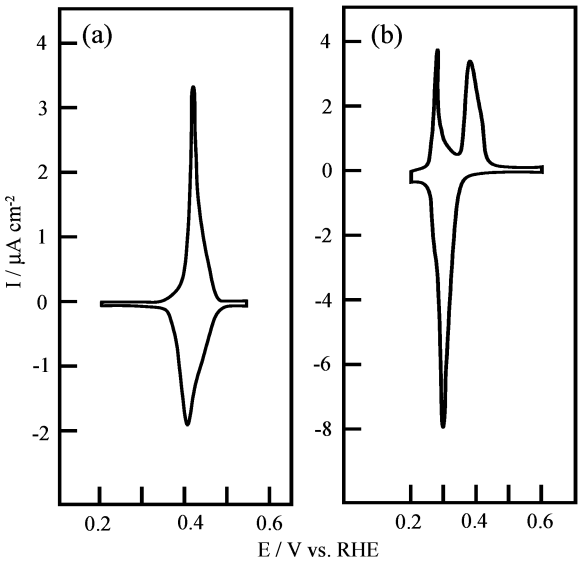

Figure 1. CV of Au(100) electrode modified with irreversibly adsorbed SbO^+ in 0.1 M $HClO_4$; scan rate, 2 mV s^{-1} (part a). CV of Au(100) electrode in 50 μM Sb_2O_3 + 0.1 M $HClO_4$; scan rate, 1 mV s^{-1} (part b).

CVs recorded in a $HClO_4$ solution containing Sb(III) were different from the CV in Figure 1a. Figure 1b shows a CV obtained on Au(100) in a 0.1 M $HClO_4$ solution containing 50 μM Sb_2O_3. The electrode potential was initially scanned from 0.7 V in the negative direction at the scan rate of 2 mV s^{-1}. In the negative scan, the reduction peak of SbO^+ at 0.4 V, which is seen in Figure 1a, was not observed; instead, a new, very sharp peak appeared at 0.30 V. In the subsequent positive scan, two peaks were observed at 0.28 and 0.4 V. The peak at 0.28 V is much sharper than that at 0.4 V. The shape of the CV shown in Figure 1b was steadily obtained upon repetition of potential cycles. The charge consumed for the cathodic peak was calculated to be approximately 365 μC cm^{-2}, whereas the charges for the two anodic peaks at 0.28 and 0.4 V were approximately 155 and 205 μC cm^{-2}, respectively. The sum of the charges of the two anodic peaks was nearly equal to the charge of the cathodic UPD peak. Similar CVs to that in Figure 1b were also reported at Au(100) in Sb_2O_3 + H_2SO_4.[33,37] We mentioned already that SbO^+ is irreversibly adsorbed on Au(100) and that the redox reaction of SbO^+ occurs at 0.4 V. Because the charge density of the redox reactions for the adsorbed SbO^+ was only 135 μC cm^{-2} (Figure 1a), the simultaneous UPD of Sb must be assumed to take place at this cathodic peak to account for the charge density of 365 μC cm^{-2}, in agreement with previous results.[33,37]

The theoretical total charge corresponding to the formation of a complete (1×1) monolayer of Sb on Au(100) is 579 μC

cm^{-2}, assuming that SbO^+ on the surface or in solution is reduced to Sb^0 on Au(100) during the cathodic potential scan. Using the values listed already, the surface coverage of Sb after the cathodic peak was calculated to be 0.63. Because the coverage of SbO^+ was calculated to be 0.24, as already described, the UPD contributed to the increase in coverage by 0.39. Sb coverages on Au(100) after the cathodic peak were reported to be much smaller in $Sb_2O_3 + H_2SO_4$.[33,37] As has been discussed in detail,[41,42] the UPD processes of Sb should also be influenced significantly by electrolyte anions.

It was reported that the first cathodic peak, observed at 0.28 V in this study (Figure 1b), should be mainly associated with the desorption of Sb from Au(100) and the second peak at 0.4 V mainly with the oxidation of Sb to SbO^+ on Au(100).[33] This can be understood by comparing Figure 1a and b, because the potential for the oxidation peak of Sb to SbO^+, 0.4 V in Figure 1a, agrees very well with that for the second anodic peak in Figure 1b. In the following section, the results of in situ STM study will be presented to support the association of the first anodic peak at 0.28 V in Figure 1b with the desorption of Sb. After the partial anodic desorption of Sb at approximately 0.3 V, the coverage of Sb on Au(100) was calculated to be 0.35. In the second anodic peak, Sb atoms of 0.11 in coverage might be desorbed from the surface and those of 0.24 in coverage could be oxidized to SbO^+ on the surface, which will also be discussed.

In Situ STM of the Adlayer of Irreversibly Adsorbed Sb on Au(100) in $HClO_4$. In this section, we report the adlayer structure of SbO^+ on Au(100) and the structure formed after the reduction.

Figure 2a shows an STM image acquired at 0.5 V in 0.1 M $HClO_4$ after an Au(100) specimen was treated in a 50 μM Sb_2O_3 + 0.1 M $HClO_4$ solution at 0.4 V for 1 min. In Figure 2a, the steps are winding, as are those at bare Au(100), but they contain many kinks attributable to the existence of adsorbates. It is clearly seen that the terraces are covered with clusters, each of which consists of four spots. Between the clusters, individual small spots are also seen. We assign these individual spots, as well as the spots forming clusters, to SbO^+ species, as previously proposed.[34] On the surface of Au(111), domains of SbO^+ are networked,[34] but on Au(100), terraces are rather uniformly covered with SbO^+. Figure 2b shows a high-resolution image of the adlayer of SbO^+. A cluster consisting of four SbO^+ species is marked by a solid square. The sides of all clusters are in the directions of the substrate Au lattice, and the length of a side is measured at 0.52 ± 0.03 nm, which is slightly shorter than twice the Au−Au distance, 0.58 nm. Interestingly, the distance between SbO^+ species was reported to be 0.49 ± 0.01 nm on Au(111),[34] which is nearly equal to that on Au(100). Figure 3 shows a schematic illustration of the SbO^+ adlayer derived from the upper part of Figure 2b. In this model, about 60% of the SbO^+ species form clusters, as indicated by solid squares. We placed SbO^+ species forming clusters near 4-fold sites (Figure 3). Some of the SbO^+ species not forming clusters are placed separately at 4-fold sites, but some SbO^+ species are found to interact with neighboring SbO^+ so that they are moved away from 4-fold sites (Figure 3). The distance between those interacting SbO^+ species varies from 0.48 to 0.55 nm. Although an attractive interaction had also been reported previously between SbO^+ species on Au(111),[34,35] the formation of SbO^+ clusters on Au was first observed in this study on Au(100) (Figures 2 and 3). The structure of SbO^+ can be denoted as quasi (2 × 2). From the number of SbO^+ species counted in the STM images, the coverage was derived as being

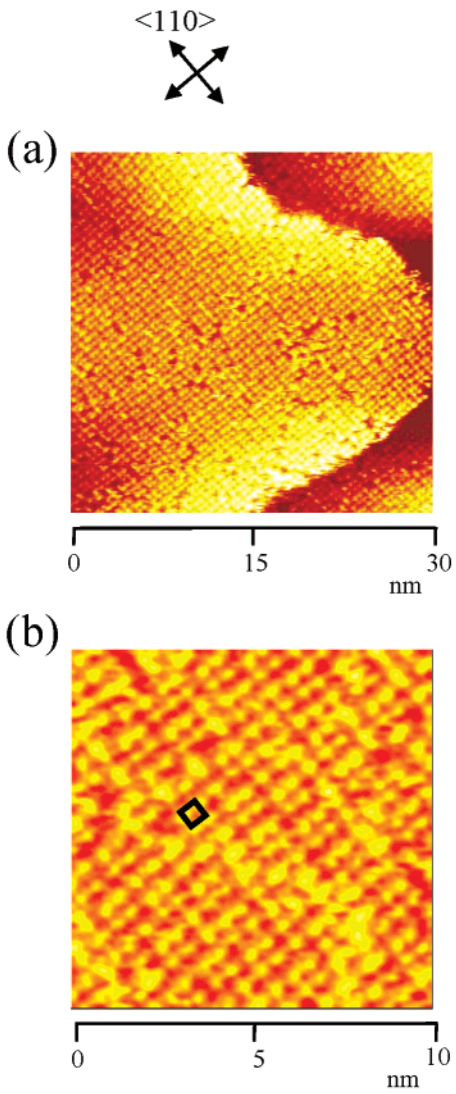

Figure 2. STM top view recorded on SbO^+-modified Au(100) in 0.1 M $HClO_4$; scan area, 30 × 30 nm^2; electrode potential, 0.5 V; tip potential, 0.3 V; tunneling current, 5 nA (part a). High-resolution STM image of SbO^+-modified Au(100) in 0.1 M $HClO_4$; scan area, 10 × 10 nm^2; electrode potential, 0.5 V; tip potential, 0.35 V; tunneling current, 5 nA (part b).

equal to 0.25. This coverage agrees with that obtained from the CV (Figure 1), 0.24, indicating that all SbO^+ species are electrochemically reduced/oxidized on Au(100) in the potential range between 0.3 and 0.5 V (Figure 1a).

When SbO^+ was electrochemically reduced to Sb during the cathodic scan to 0.3 V, the positions of individual Sb species remained unchanged; thus, the SbO^+ species were reduced at their original sites without diffusion. When the potential was scanned back in the anodic direction to 0.5 V, no change in the adlayer structure was observed.

In Situ STM of the Adlayers of Sb on Au(100) in $HClO_4$ Containing Sb(III). Now that we understand the adlayer of irreversibly adsorbed SbO^+ on Au(100) at different potentials, we will now discuss the adlayer structure of Sb on Au(100) associated with UPD. We first carried out STM measurements on Au(100) in a 50 μM Sb_2O_3 + 0.1 M $HClO_4$ solution at 0.4 V, a potential more anodic than the cathodic peak observed in Figure 1b. The quasi (2 × 2) adlayer structure of SbO^+, which we observed on the SbO^+-modified Au(100) in pure $HClO_4$ (Figures 2 and 3), was also found in $HClO_4$ containing Sb(III) with the same coverage of 0.25. Then, the potential was stepped

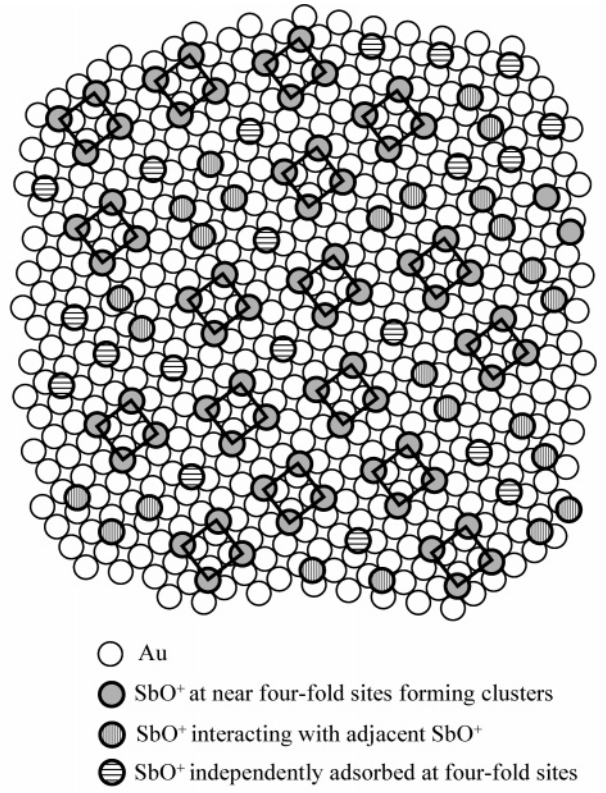

Figure 3. Schematic representation of SbO^+-modified Au(100).

to a value more cathodic than that of the cathodic peak (Figure 1b). In the first minute after stepping the potential to 0.25 V, those steps that had been winding (Figure 2a) became straight. The large-scale STM image acquired at 0.25 V (Figure 4a) shows that the monatomic steps now run parallel to the ⟨001⟩ direction, rotated by 45° with respect to the atomic rows of the substrate. On the terraces, dark straight belts, 1 nm in width and 5−20 nm in length, are also seen in the ⟨001⟩ direction. The same surface morphological change was reported by Yan and co-workers in H_2SO_4.[37] When we continued scanning in the same area, we observed the movement of the belts forward and sideward, which will be explained later in this section. In the high-resolution STM image shown in Figure 4b, it can be clearly seen that the spots with two different levels of brightness are aligned in the ⟨001⟩ direction. Dark belts are also seen in the center and along the left-hand side of Figure 4b. Those spots can be assigned to deposited Sb atoms with different corrugation heights at different sites. Solid lines in Figure 4b outline the unit cell. Four bright spots are seen at the corners of the unit cell, while darker spots are seen in the middle of the longer sides. The shorter sides are in the ⟨001⟩ direction, whereas the longer sides are tilted by 72° with respect to the shorter sides. The average lengths of the sides of the unit cell are 0.41 nm ($\sqrt{2}$ times the Au−Au distance) and 0.65 nm ($\sqrt{5}$ times the Au−Au distance), respectively. The results described here suggest that the Sb adlayer on Au(100) at 0.25 V has $\begin{pmatrix} 1 & 1 \\ -1 & 2 \end{pmatrix}$ symmetry. A structural model is shown in Figure 4c. The dark and bright spots in Figure 4b are now assigned to Sb atoms at 4-fold hollow sites and bridge sites, respectively. The structure of the very dark belts seen in Figure 4a,b is not apparent, although rows of spots are seen even on these belts. The distance between two bright Sb rows sandwiching the dark belts was 1.46 nm, not equal to 2 but approximately 2.4−2.5 times the distance between two bright Sb rows in the ordered $\begin{pmatrix} 1 & 1 \\ -1 & 2 \end{pmatrix}$ structure (Figure 4b,c). Because the brightness of the two bright

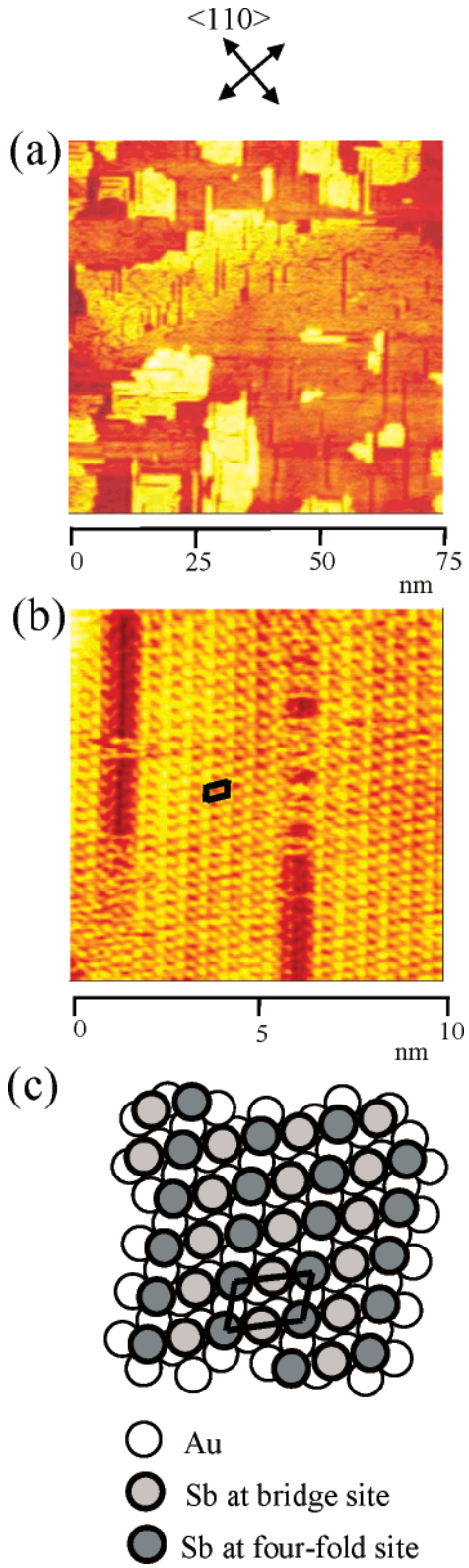

Figure 4. STM top view recorded at a potential after the cathodic peak on Au(100) in 0.1 M $HClO_4$ + 50 μM Sb_2O_3; scan area, 75 × 75 nm^2; electrode potential, 0.25 V; tip potential, 0.35 V; tunneling current, 5 nA (part a). High-resolution STM image recorded at a potential after the cathodic peak on Au(100) in 0.1 M $HClO_4$ + 50 μM Sb_2O_3; scan area, 10 × 10 nm^2; electrode potential, 0.25 V; tip potential, 0.35V; tunneling current, 20 nA (part b). Structure model for an Sb adlayer deposited on Au(100) forming a $\begin{pmatrix} 1 & 1 \\ -1 & 2 \end{pmatrix}$ structure (part c).

rows sandwiching the dark belts is the same as that of the other bright rows in the ordered area, it is naturally considered that

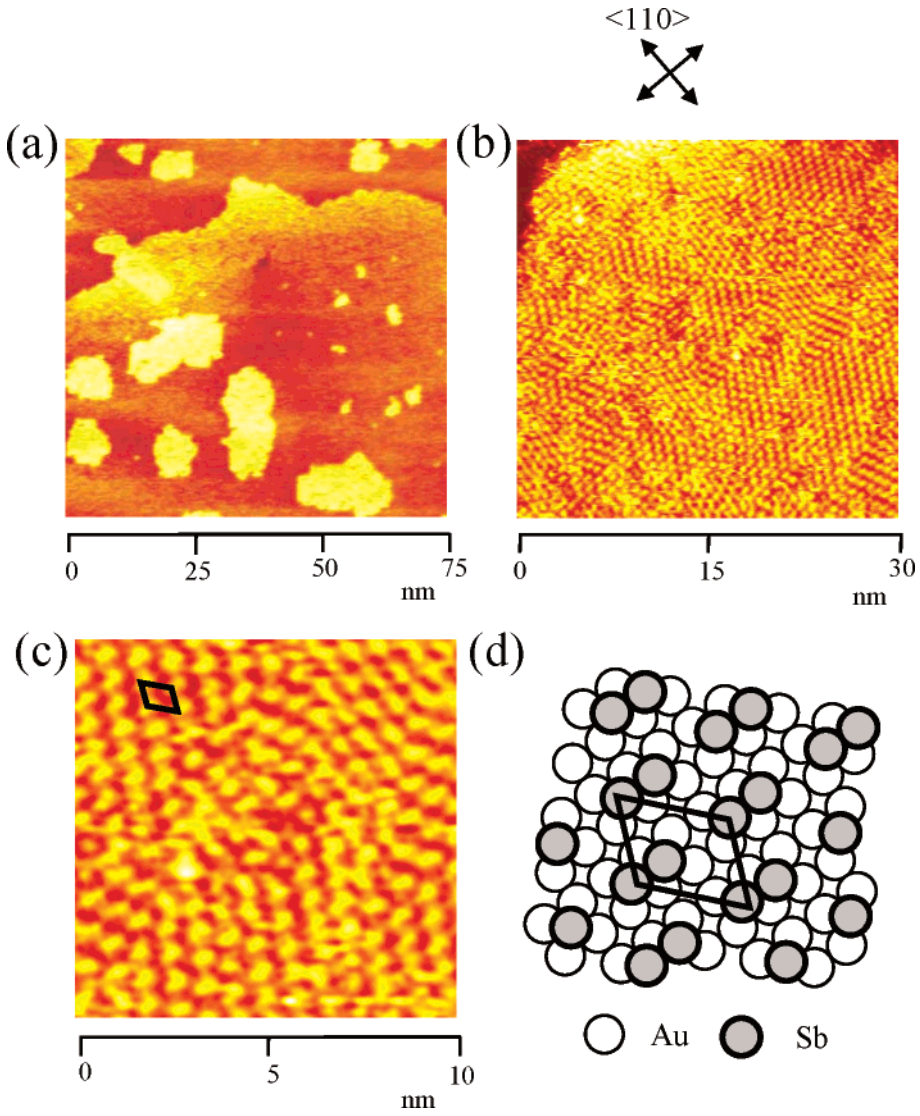

Figure 5. Large-scale STM image of Au(100) in 50 μM Sb_2O_3 + 0.1 M $HClO_4$; scan area, 75 × 75 nm^2; electrode potential, 0.3 V; tip potential, 0.4 V; tunneling current, 5 nA (part a). STM top view of Sb on Au(100) in 50 μM Sb_2O_3 + 0.1 M $HClO_4$; scan area, 30 × 30 nm^2; electrode potential, 0.3 V; tip potential, 0.25 V; tunneling current, 30 nA (part b). High-resolution STM image of Sb adlayer on Au(100) in 50 μM Sb_2O_3 + 0.1 M $HClO_4$; scan area, 10 × 10 nm^2; electrode potential, 0.3 V; tip potential, 0.25 V; tunneling current, 30 nA (part c). Structure model for Sb adlayer deposited on Au(100) with a $\begin{pmatrix} 2 & 1 \\ -2 & 2 \end{pmatrix}$ unit cell (part d).

those Sb atoms are also adsorbed at bridge sites, but they are pushed aside to widen the belt. Consequently, the surface density of the Sb atoms in the belts becomes lower than the density in the ordered $\begin{pmatrix} 1 & 1 \\ -1 & 2 \end{pmatrix}$ structure. Considering the van der Waals diameter of Sb, 0.29 nm, and the nearest-neighbor distance of Sb on Au(100) after the UPD forming $\begin{pmatrix} 1 & 1 \\ -1 & 2 \end{pmatrix}$, 0.32 nm, it is understandable that the distance between Sb atoms on Au(100) is almost minimized in this UPD layer. The arrangement of Sb atoms in the $\begin{pmatrix} 1 & 1 \\ -1 & 2 \end{pmatrix}$ adlayer (Figure 4), however, is very different from that in a crystalline structure; thus, a surface tension should exist in the UPD adlayer. The dark belts might exist in the Sb adlayer to compensate the surface tension and lower the total surface energy. While scanning, these dark belts were observed to move slightly, as mentioned already. The belts moved sideward by a distance of an atom without changing their width; the Sb atoms underwent rearrangement. They also grew forward and backward with the changing arrangement of Sb atoms at the apexes. This movement of dark belts was induced, at least partly, by the scanning of the STM tip, because as the tunneling current increased, movement of the dark belts became more frequently observed.

From the charge density for the cathodic peak observed in Figure 1b, the coverage of Sb was calculated to be 0.63. Because the structure of the dark belts (Figure 4a,b) has not been fully elucidated, some ambiguity exists in the estimation of the Sb coverage from the STM results. From the adlayer model (Figure 4c) without considering the existence of the dark belts, the coverage of Sb can be calculated as 0.66, which does not contradict the CV result, 0.63.

Now, the electrode potential was stepped in the anodic direction to 0.3 V, a potential more anodic than the first anodic peak with a charge density of 155 μC cm^{-2} (Figure 1b). The STM image in Figure 5a was obtained in the same area where the image in Figure 4a had been observed. The straight steps (Figure 4a, 0.25 V) now became winding (Figure 5a, 0.30 V). After the potential step, no 3D islands or pits were seen, while the dark belts observed at 0.25 V (Figure 4a,b) completely disappeared. A close-up view of a terrace in Figure 5b shows that the surface is covered with spots with the same brightness. The domains are small, about 5−10 nm in size. The high-resolution STM image is shown in Figure 5c. Spots in one domain appear to be elongated in the same direction or the

direction of the substrate Au lattice. Detailed examination of the STM images revealed that each elongated spot consists of two small spots. A unit cell is outlined in Figure 5c by solid lines. The longer sides of the unit cell are in the ⟨001⟩ direction, whereas the shorter sides are tilted by 72° with respect to the longer sides. The average lengths of the sides of the unit cell are 0.8 nm ($2\sqrt{2}$ times the Au−Au distance) and 0.65 nm ($\sqrt{5}$ times the Au−Au distance), respectively. The results described here suggest that the Sb adlayer at 0.30 V on the Au(100) surface takes a $\begin{pmatrix} 2 & 1 \\ -2 & 2 \end{pmatrix}$ structure, whose model is depicted in Figure 5d. All surface species are placed at 4-fold sites. The coverage of the surface species is 0.34 in this model (Figure 5d).

For the first anodic peak at 0.28 V (Figure 1b), the possible reaction is either desorption of Sb from the surface into solution, oxidation of Sb to SbO^+ on the surface, or a combination of both. It was reported that this anodic peak is mainly due to the desorption of Sb from Au surface.[33,37] If the charge for this first anodic peak, 155 μC cm^{-2}, is assumed to be consumed only by the electrochemical desorption of Sb, all surface species will be Sb atoms, with a coverage of 0.35, as already discussed in the CV section. As described already, the coverage of the surface species derived from the STM images is 0.34 (Figure 5). Therefore, it is probable that at the first anodic peak, Sb atoms are desorbed from the surface and the remaining Sb atoms formed the $\begin{pmatrix} 2 & 1 \\ -2 & 2 \end{pmatrix}$ structure. It is very interesting to note that this $\begin{pmatrix} 2 & 1 \\ -2 & 2 \end{pmatrix}$ structure was also formed after the potential step from 0.4 V directly to 0.3 V. This result implies that the kinetics explains the reason for the existence of only one cathodic peak in the CV (Figure 1b); thermodynamically, two different adlayer structures of Sb could exist on Au(100) at different electrode potentials. However, more direct evidence is necessary to determine the composition of the surface species.

After the potential was swept from 0.3 to 0.4 V, a quasi (2 × 2) structure was again formed because of the stripping of Sb amounting to a corresponding coverage of 0.11 and the oxidation of Sb to SbO^+ on the surface with a corresponding coverage of 0.24.

Electroreduction of H_2O_2 on Sb-Modified Au(100). Voltammetric measurements were next carried out in a solution of 50 μM Sb_2O_3 + 0.1 M $HClO_4$ + 10 mM H_2O_2 to investigate the relationship between the adlayers of Sb species and the electroreduction of H_2O_2 on Au(100). The current−potential curves for the H_2O_2 reduction on Au(100) are shown in Figure 6. The dotted line in Figure 6 represents the current−potential curve obtained on Au(100) in 0.1 M $HClO_4$ + 10 mM H_2O_2 for comparison. As the potential was swept from 0.7 V in the cathodic direction, the reduction current of H_2O_2 gradually increased up to approximately 100 μA cm^{-2} at 0.1 V. The solid and dashed lines are current−potential curves obtained in the cathodic and anodic directions, respectively, in 50 μM Sb_2O_3 + 0.1 M $HClO_4$ + 10 mM H_2O_2. The cathodic curve in 50 μM Sb_2O_3 + 0.1 M $HClO_4$ + 10 mM H_2O_2 (solid line in Figure 6) exhibited a sharp peak at 0.3 V, and the H_2O_2 reduction current reached a maximum of approximately 700 μA cm^{-2}. The H_2O_2 reduction current decreased rapidly at potentials more negative than 0.30 V, reaching approximately 200 μA cm^{-2} at 0.2 V. The anodic current (dashed line in Figure 6) decreased at 0.3 V, and a peak appeared again at 0.4 V. Compared with the CV in Figure 1b, these results clearly show that the H_2O_2 reduction reaction is significantly influenced by the adlayers of Sb species. Examining the current at 0.4 V in the cathodic scan shows that the adlayer of SbO^+ does not enhance the reduction of H_2O_2 very much. At the potential for the cathodic peak in the cathodic scan for the reduction of SbO^+ and the UPD of Sb at 0.3 V in Figure 1b, the H_2O_2 reduction rate is highly enhanced. From the anodic scan in Figure 6, it is understood that both $\begin{pmatrix} 1 & 1 \\ -1 & 2 \end{pmatrix}$ and $\begin{pmatrix} 2 & 1 \\ -2 & 2 \end{pmatrix}$ adlayers exhibit activity for the reduction of H_2O_2. The enhancement of the reduction of H_2O_2 was observed also on Au(111).

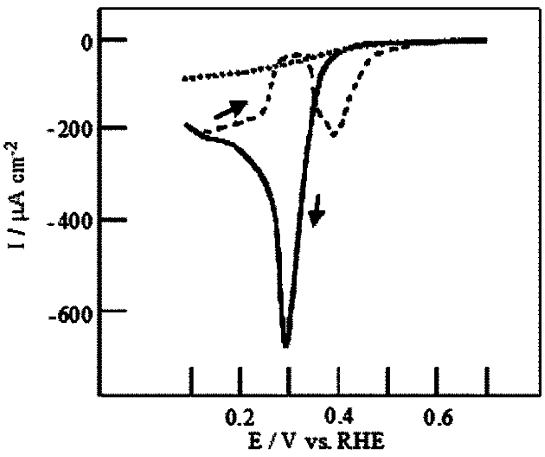

Figure 6. Current−potential curves of Au(100) electrode. Dotted line (···): cathodic sweep in 0.1 M $HClO_4$ + 10 mM H_2O_2; scan rate, 1 mV s^{-1}. Solid line (−): cathodic sweep in 50 μM Sb_2O_3 + 0.1 M $HClO_4$ + 10 mM H_2O_2; scan rate, 1 mV s^{-1}. Dashed line (- - -): anodic sweep in 50 μM Sb_2O_3 + 0.1 M $HClO_4$ + 10 mM H_2O_2; scan rate, 1 mV s^{-1}.

Li and Gewirth suggested, from their study of the mechanism of the H_2O_2 electroreduction on the Bi-modified Au(111) surface using DFT calculations, that the O atoms in H_2O_2 interact strongly with two Bi atoms and cleavage of the O−O bond arises because of the distance between adjacent Bi adatoms on the Au(111) surface.[4] According to their suggestion, the decrease in the distance between Bi adatoms with increasing coverage causes a decrease in the catalytic activity for the electroreduction of H_2O_2. Their suggested mechanism might explain the observed enhancement of the rate of H_2O_2 reduction on $\begin{pmatrix} 1 & 1 \\ -1 & 2 \end{pmatrix}$ and $\begin{pmatrix} 2 & 1 \\ -2 & 2 \end{pmatrix}$ adlayers. What is most pronounced, however, is the reaction enhancement at 0.3 V in the cathodic sweep. At this potential, the processes of the reduction of SbO^+ and the adsorption of Sb could not be distinguished from each other in the present study. Moreover, the transient adlayer structure during the cathodic scan could not be observed by STM.

We also carried out the H_2O_2 reduction reaction on a SbO^+-modified Au(111) surface in 0.1 M $HClO_4$ + 10 mM H_2O_2 without Sb_2O_3 and found that the enhancement was much smaller than in the solution containing Sb_2O_3. Further study is required to understand this large reaction enhancement at 0.3 V in the cathodic sweep.

Conclusion

The adlayers of Sb species on Au(100) were investigated in $HClO_4$ solution by in situ STM and electrochemical measurements. It was shown that the irreversibly adsorbed SbO^+ formed a quasi (2 × 2) structure. Two adlayer structures of Sb atoms, $\begin{pmatrix} 2 & 1 \\ -2 & 2 \end{pmatrix}$ and $\begin{pmatrix} 1 & 1 \\ -1 & 2 \end{pmatrix}$, were observed at 0.30 and 0.25 V. respectively. The electroreduction of H_2O_2 was significantly influenced by the adlayers of Sb species.

Acknowledgment. This work was supported partially by the COE project, Giant molecules and Complex Systems, 2004, from the Ministry of Education, Culture, Sports, Science and Technology, Japan, and by Core Research for Evolutional Science and Technology organized by the Japan Science and

Technology Agency. The authors thank Dr. Y. Okinaka for his help in writing this manuscript.

References and Notes

(1) Tarasevich, M. R.; Sadkowski, A.; Yeager, E. *Compr. Treatise Electrochem.* **1983**, *7*, 301−398.
(2) Adzic, R. In *Electroanalysis*; Lipkowski, J., Ross, P. N., Eds.; Wiley-VCH: New York, 1998; pp 197−242.
(3) Markovic, N. M.; Schmidt, T. J.; Stamenkovic, V.; Ross, P. N. *Fuel Cells* **2001**, *1*, 105−116.
(4) Li, X.; Gewirth, A. A. *J. Am. Chem. Soc.* **2003**, *125*, 7086−7099.
(5) Jüttner, K. *Electrochim. Acta* **1984**, *29*, 1597−1604.
(6) Jüttner, K. *Electrochim. Acta* **1986**, *31*, 917−927.
(7) Kokkindis, G. *J. Electroanal. Chem.* **1986**, *201*, 217−236.
(8) Sayed, S. M.; Jüttner, K. *Electrochim. Acta* **1983**, *28*, 1635−1641.
(9) Alvarez-Rizatti, M.; Jüttner, K. *J. Electroanal. Chem.* **1983**, *144*, 351−363.
(10) Adzic, R. R.; Tripkovic, A. V.; Markovic, N. M. *J. Electroanal. Chem.* **1980**, *114*, 37−51.
(11) Adzic, R.; Tripkovic, A.; Atanasoski, R. *J. Electroanal. Chem.* **1978**, *94*, 231−235.
(12) Kokkinidis, G.; Sazou, D. *J. Electroanal. Chem.* **1986**, *199*, 165−176.
(13) Amadelli, R.; Molla, J.; Bindra, P.; Yeager, E. *J. Electrochem. Soc.* **1981**, *128*, 2706−2709.
(14) Amadelli, R.; Markovic, N.; Adzic, R.; Yeager, E. *J. Electroanal. Chem.* **1983**, *159*, 391−412.
(15) Green, M. P.; Hanson, K. J.; Carr, R.; Lindau, I. *J. Electrochem. Soc.* **1990**, *137*, 3493−3497.
(16) Green, M. P.; Hanson, K. J. *Surf. Sci. Lett.* **1991**, *259*, L743−L749.
(17) Tao, N. J.; Pan, J.; Li, Y.; Oden, P. I.; DeRose, J. A.; Lindsay, S. M. *Surf. Sci. Lett.* **1992**, *271*, L338−L344.
(18) Chen, C.-H.; Gewirth, A. A. *J. Am. Chem. Soc.* **1992**, *114*, 5439−5440.
(19) Chen, C.-H.; Kepler, K. D.; Gewirth, A. A.; Ocko, B. M.; Wang, J. *J. Phys. Chem.* **1993**, *97*, 7290−7294.
(20) Oh, I.; Biggin, M. E.; Gewirth, A. A. *Langmuir* **2000**, *16*, 1397−1406.
(21) Solomun, T.; Kautek, W. *Electrochim. Acta* **2001**, *47*, 679−687.
(22) Tamura, K.; Ocko, B. M.; Wang, J. X.; Adzic, R. R. *J. Phys. Chem. B* **2002**, *106*, 3896−3901.
(23) Niece, B. N.; Gewirth, A. A. *Langmuir* **1996**, *12*, 4909−4913.
(24) Hara, M.; Nagahara, Y.; Yoshimoto, S.; Inukai, J.; Itaya, K. *J. Electrochem. Soc.* **2004**, *151*, E92−E96.
(25) Hara, M.; Nagahara, Y.; Yoshimoto, S.; Inukai, J.; Itaya. K. *Jpn. J. Appl. Phys.* **2004**, *43*, 7232−7233.
(26) Polewska, W.; Wang, J. X.; Ocko, B. M.; Adzic, R. R. *J. Electroanal. Chem.* **1994**, *376*, 41−47.
(27) Adzic, R. R.; Wang, J. X.; Ocko, B. M. *Electrochim. Acta* **1995**, *40*, 83−89.
(28) Schmidt, U.; Vinzelberg, S.; Staikov, G. *Surf. Sci.* **1996**, *348*, 261−279.
(29) Hachiya, T.; Honbo, H.; Itaya, K. *J. Electroanal. Chem.* **1991**, *315*, 275−291.
(30) Sashikata, K.; Furuya, N.; Itaya, K. *J. Electroanal. Chem.* **1991**, *316*, 361−368.
(31) Abe, T.; Miki, Y.; Itaya, K. *Bull. Chem. Soc. Jpn.* **1994**, *67*, 2075−2078.
(32) Abe, T.; Swain, G. M.; Sashikata, K.; Itaya, K. *J. Electroanal. Chem.* **1995**, *382*, 73−83.
(33) Jung, G.; Rhee, C. K. *J. Electroanal. Chem.* **1997**, *436*, 277−280.
(34) Jung, C.; Rhee, C. K. *J. Electroanal. Chem.* **2004**, *566*, 1−5.
(35) Wu, Q.; Shang, W. H.; Yan, J. W.; Xie, Z. X.; Mao, B. W. *J. Phys. Chem. B* **2003**, *107*, 4065−4069.
(36) Wu, Q.; Shang, W. H.; Yan, J. W.; Mao, B. W. *J. Mol. Catal. A: Chem.* **2003**, *199*, 49−56.
(37) Yan, J. W.; Wu, Q.; Shang, W. H.; Mao, B. W. *Electrochem. Commun.* **2004**, *6*, 843−848.
(38) Clavilier, J.; Faure, R.; Guinet, G.; Durand, R. *J. Electroanal. Chem.* **1980**, *107*, 205−209.
(39) Dakkouiri, A. S.; Kolb. D. M. In *Interfacial Electrochemistry*; Wieckowski, A., Ed.; Marcel Dekker: New York, 1999; pp 151−173.
(40) Cotton, F. A. *Advanced Inorganic Chemistry*; Wiley: New York, 1972.
(41) Itaya, K. *Prog. Surf. Sci.* **1998**, *58*, 121−248.
(42) Magnussen, O. M. *Chem. Rev.* **2002**, *102*, 679−726.